Different Response to Cd2+ Adsorption by Alkali-modified Biochars Derived From Soybean Straw and Rape Straw

Yaxin Kang
Nanjing Agricultural University - Weigang Campus: Nanjing Agricultural University
Yi Zhou
Nanjing Agricultural University - Weigang Campus: Nanjing Agricultural University
Hao Li
Nanjing Agricultural University - Weigang Campus: Nanjing Agricultural University
Shanguo Chen
Nanjing Agricultural University - Weigang Campus: Nanjing Agricultural University
Fenghua Tian
Nanjing Agricultural University - Weigang Campus: Nanjing Agricultural University
Lianqing Li (lqli@njau.edu.cn)
Nanjing Agricultural University - Weigang Campus: Nanjing Agricultural University
https://orcid.org/0000-0003-1656-1235
Marios Drosos
Nanjing Agricultural University - Weigang Campus: Nanjing Agricultural University
Stephen Joseph
Nanjing Agricultural University - Weigang Campus: Nanjing Agricultural University
Genxing Pan
Nanjing Agricultural University - Weigang Campus: Nanjing Agricultural University

Research Article

Keywords: Biochar, Cadmium, Alkali modification, Adsorption mechanism

Posted Date: April 5th, 2021

DOI: https://doi.org/10.21203/rs.3.rs-167467/v1

Different response to Cd^{2+} adsorption by alkali-modified biochars derived from soybean straw and rape straw

Yaxin Kang [a], Yi Zhou [a], Hao Li [a], Shanguo Chen [a], Fenghua Tian [a], Lianqing Li [a,*], Marios Drosos [a], Stephen Joseph [a,b], Genxing Pan [a]

[a] Institute of Resources, Ecosystem and Environment of Agriculture and Center of Biochar and Green Agriculture, Nanjing Agricultural University, 1 Weigang, Nanjing 210095, China

[b] School of Materials Science and Engineering, University of New South Wales, Sydney, NSW 2052, Australia

* Corresponding author at: Institute of Resources, Ecosystem and Environment of Agriculture and Center of Biochar and Green Agriculture, Nanjing Agricultural University, 1 Weigang, Nanjing 210095, China.
Tel/Fax: +86 25 84398657
E-mail address: lqli@njau.edu.cn (L. Li).

Abstract

Biochars have been modified by alkali ($Ca(OH)_2$) to enhance Cd sorption capacity in aqueous solution. In this research, the alkali-modified (Ca) biochars were prepared by co-pyrolyzing lime ($Ca(OH)_2$) and soybean straw (SBB) or rape straw (RSB) at 450 °C. The absorption mechanism was investigated by a series of experiments and was provided by quantitative analysis. The maximum adsorption capacities of Cd^{2+} by Ca-SBB and Ca-RSB were calculated to be 78.49 mg g^{-1} and 49.96 mg g^{-1}, which were 1.56 and 1.48 times higher than SBB (50.40 mg g^{-1}) and RSB (33.79 mg g^{-1}), respectively. Compared with the original biochar (SBB, RSB), alkali-modified biochars (Ca-SBB and Ca-RSB) were found to have faster adsorption kinetics and lower desorption efficiencies. The mechanism study indicated that $Ca(OH)_2$ modification effectively enhanced the contribution of ion exchange and decreased the contribution of functional groups complexation. After $Ca(OH)_2$ modification, precipitation and ion exchange mechanisms dominated Cd^{2+} absorption on Ca-SBB, accounting for 49.85% and 34.94% of the total adsorption, respectively. Similarily ion exchange and precipitation were the main adsorption mechanism on Ca-RSB, accounting however for 61.91% and 18.47% of total adsorption, respectively. These results suggested that alkali-modified biochars have great potential in adsorbing cadmium in wastewater.

Keywords：Biochar ; Cadmium ; Alkali modification ; Adsorption mechanism

1. Introduction

Cadmium (Cd) is one of the most toxic inorganic pollutants in wastewater and soil because of its strong migration and enrichment ability, which causes severe damage to human health (Patar, et al. 2016). Several technologies have been used to remove Cd from wastewater and soil solution such as precipitation, complexation and adsorption (Bolan, et al. 2014; Fu and Wang 2011). Considering the removal efficiency, easy operation and secondary pollution, adsorption method is considered to be the best one (Burakov, et al. 2018).

Biochar, a solid product prepared by biomasses pyrolysis under oxygen-limited conditions (Lehmann 2007), has been reported to sequestrate carbon, improve soil quality and increase crop yield (Lehmann 2007; Woods, et al. 2006; Zhang, et al. 2010). The deepening of biochar research revealed its great potential in the treatment of heavy metal pollution in water and soil, due to its well-developed pore structure, generally high pH, abundant oxygen-containing functional groups and mineral components (Ahmad, et al. 2014; Bian, et al. 2014; Li, et al. 2017). Cd absorption capacity of biochar estimated to be 0.3-39.1 mg g^{-1} (Inyang, et al. 2016). Biochar soil amendment was found consistently and significantly to increase soil pH and decrease soil extractable Cd over a 3-year period experiment (Bian, et al. 2014). Based on the current research, the Cd^{2+} adsorption mechanisms on biochar included metal ion exchange, mineral precipitation, functional groups complexation and Cd^{2+}-π coordination (Trakal, et al. 2014; Wang, et al. 2018; Yu, et al. 2018; Zhang, et al. 2015).

Though biochar is an environmentally friendly adsorbent for Cd removal from water, the Cd^{2+} absorption capacity of biochar is generally lower compared with other bio sorbents such as activated carbon (Inyang, et al. 2016; Wilson, et al. 2006). In order to improve its adsorption performance, it

67 is necessary to modify it through loading with minerals, organic functional groups, nano-particles
68 and activation with alkali solutions (Ahmed, et al. 2016). In all modification methods, loading
69 minerals on the surface of biochar is the most promising one, combining the advantages of biochar
70 and minerals (Tan, et al. 2016). Lime ($Ca(OH)_2$) is the most common passivator used to remove
71 Cd^{2+} from wastewater and soil solution, due to its affordable price and availability (Fu and Wang
72 2011). Therefore, in order to reduce the cost and improve the Cd adsorption performance, co-
73 pyrolysis of straw and $Ca(OH)_2$ is a feasible and easy-to-operate method. Biochar prepared by co-
74 pyrolysis of $Ca(OH)_2$ and sludge improved the surface area, DOC content and alkalinity (Ren, et al.
75 2018). However, there is still a lack of quantitative research on the relative distribution of Cd^{2+}
76 adsorption mechanisms in alkali-modified biochar.

77 In this study, the alkali-modified biochars were prepared by co-pyrolyzing lime ($Ca(OH)_2$) and
78 straw (rape straw or soybean straw), and were then used to quantify Cd^{2+} adsorption and reveal its
79 binding mechanism. The purposes of the study are 1) to investigate the Cd adsorption
80 performance and the contribution of different binding mechanisms of alkali-modified biochars
81 produced from rape straw and soybean straw, respectively; and 2) to compare the different response
82 to Cd^{2+} adsorption by two kinds of alkali-modified biochars.

83 2. Materials and methods

84 2.1. Materials

85 Rape straw and soybean straw were collected from an agricultural market in Nanjing. All
86 chemicals were of analytical grade and all solutions were made with deionized water (DI). Cadmium
87 nitrate ($Cd(NO_3)_2 \cdot 4H_2O$) and sodium nitrate ($NaNO_3$) were purchased from Aladdin Biochemical
88 Technology Co. , Ltd, Shanghai, China. Lime ($Ca(OH)_2$) was purchased from Xilong Scientific Co.,

89 Ltd, Guangdong, China.

90 2.2. Biochar preparation

91 The dried rape and soybean straw were placed in a stainless steel reactor and heated in a muffle
92 furnace under oxygen-limited condition at 450℃ for 2 h. The biochars originated from rape straw
93 and soybean straw were referred to as RSB and SBB, respectively. The alkali-modified biochars
94 were prepared by heating rape straw or soybean straw together with lime ($Ca(OH)_2$) at 450 ℃ for 2
95 h. Specifically, alkali-modified biochars were originated from rape straw or soybean straw mixed
96 with $Ca(OH)_2$ in a ratio of 1:0.028 (straw/Ca, w/w). The alkali-modified biochars derived from rape
97 straw and soybean straw were referred to as Ca-RSB and Ca-SBB, respectively. The tested biochars
98 were ground and passed through 0.5-mm sieve for later testing. The biochar samples were
99 demineralized by rinsing with 1M HCl followed by washing with DI until the pH became constant
100 (Wang, et al. 2015).

101 2.3. Characterization of biochars

102 Biochars pH values were measured using a digital pH meter. Cation exchange capacity (CEC)
103 was analyzed using ammonium acetate exchange method by flame spectrophotometer (Gaskin, et
104 al. 2008), and dissolved organic carbon (DOC) was measured by total organic carbon analyzer (TOC)
105 (Jena Multi N/C 2100) at a ratio of 1.0 g biochar in 20 mL DI water after 24 h equilibrium. Total C,
106 H and N contents of biochars were determined by an elemental analyzer (Vario EL cube). The
107 content of K, Ca, Na, Mg, P and S was determined by inductively coupled plasma-optical emission
108 spectroscopy (ICP-OES) (Agilent 710). Specific surface area and pore properties of biochars were
109 measured using a surface area and porosity analyzer (Micromeritics Tristar II 3020, USA). The
110 characteristics of biochars are given in more details in Table S1.

111 The surface structure and morphology of all biochar samples were observed with a Scanning
112 Electron Microscope (SEM, ZEISS GeminiSEM 500). Surface element analysis was conducted
113 simultaneously with the SEM at the same surface locations using energy dispersive X-ray
114 spectroscopy (EDS, AZtec X-Max 50). X-ray diffraction (XRD) patterns were collected using a
115 powder X-ray diffractometer (XRD, X `Pert MPD) to determine possible mineral formation within
116 the biochar. Fourier-transform infrared (FTIR) spectra (Nicolet 8700) were also collected in the
117 400–4000 cm^{-1} range to identify the organic functional groups present in the biochars' surface.

118 2.4. Sorption experiments

119 Cadmium stock solution (1000 mg L^{-1}) was prepared by dissolving cadmium nitrate
120 ($Cd(NO_3)_2 \cdot 4H_2O$) in 0.01 mol L^{-1} $NaNO_3$ solution. Adsorption kinetics experiments were carried
121 out by adding 0.1 g biochar samples to 25 mL solutions containing 100mg L^{-1} Cd^{2+} agitated at a
122 speed of 180 rpm. Each sample was extracted at different time intervals (5, 15, 30, 60, 120, 240, 480
123 and 720 min). Sorption kinetics were evaluated at room temperature (25 °C) and the initial pH value
124 was adjusted to 5.0 ± 0.05 by adding 0.1 M HNO_3 or 0.1 M NaOH. Adsorption isotherm experiments
125 were studied with initial Cd^{2+} concentrations in the range of 10–300 mg L^{-1} at pH 5.0 for 12h.
126 Previously Cd-loaded biochars were shaken with 25 ml of 0.1 mol L^{-1} $NaNO_3$ solution as desorbing
127 agent at 25 °C for 12 h. The final suspensions were filtered by 0.45μm filter papers and the
128 supernatant solution was separated for analysis of Cd^{2+} using flame atomic absorption
129 spectrophotometer (FAAS, Persee A3, Beijing). Finally, the equilibrium sorption capacity Q_e (mg
130 g^{-1}), the equilibrium desorption capacity Q_d (mg g^{-1}) and the desorption rate (% desorption) were
131 calculated according to the following equations:

$$Q_e = (C_0 - C_e) * V/m \quad (1)$$

$$Q_d = (C_{de} - C_{d0}) * V/m \quad (2)$$

$$\%\ \text{desorption} = Q_d / Q_e * 100\% \quad (3)$$

where C_0 and C_e are the initial and equilibrium concentration (mg L^{-1}) during adsorption, and C_{d0} and C_{de} are the initial and equilibrium concentration (mg L^{-1}) during desorption, respectively. V is the volume (L) of the metal ion solution, and m is the mass (g) of biochar.

The adsorption kinetic was modeled by pseudo-first-order (Eq. (4)), pseudo-second-order (Eq. (5)) and particle diffusion kinetic equations (Eq. (6)), and the adsorption isotherm was simulated using Langmuir (Eq. (7)) and Freundlich (Eq. (8)) isotherm models:

$$Q_t = Q_e (1 - e^{-k1t}) \quad (4)$$

$$Q_t = k_2 Q_e^2 t / (1 + k_2 Q_e t) \quad (5)$$

$$Q_t = K_p t^{0.5} + C \quad (6)$$

$$Q_e / Q_{max} = BC_e / (1 + BC_e) \quad (7)$$

$$Q_e = KC_e^{1/n} \quad (8)$$

where Q_e and Q_t are the adsorption capacity (mg g^{-1}) at equilibrium and time t, respectively. k_1 (h^{-1}), k_2 (mg g^{-1} h^{-1}) and K_p (mg g^{-1} $h^{-0.5}$) indicate the rate constants corresponding to the respective kinetic model. C_e is the residual Cd^{2+} concentration (mg L^{-1}) at equilibrium. Q_{max} is the maximum adsorption capacity (mg g^{-1}); B (L mg^{-1}) and K (L g^{-1}) are the rate constants corresponding to the respective isotherm model, and n represents the degree of nonlinearity between solution concentration and adsorption.

2.5. The contribution of different adsorption mechanisms

As described in Section 2.4, 0.05g untreated-biochar and demineralized biochar were mixed with 25mL solutions containing 250mg L^{-1} Cd^{2+} , respectively. After adsorption, the concentrations

147 of K^+, Ca^{2+}, Na^+, Mg^{2+} and Cd^{2+} in the filtrate were measured by fire photometer and FAAS. The
148 biochars loaded with and without Cd^{2+} were prepared for a series of analysis such as SEM-EDS,
149 XRD and FTIR. The adsorption capacity due to mineral precipitation (Q_{cmp}), cation exchange (Q_{cme}),
150 functional groups complexation (Q_{co}), Cd^{2+}-π coordination ($Q_{c\pi}$) and the total Cd adsorption
151 capacity (Q_{ct}) were calculated according to Wang, et al. (2015) and Cui, et al. (2016). In more details:
152 (i) Most of minerals in biochars were removed by using 1 M HCl solution. The adsorption
153 capacity due to minerals Q_{cm} (mg g^{-1}) was calculated as the difference in adsorption capacity of Cd^{2+}
154 between untreated and demineralized biochars (Eq. (9)).

$$Q_{cm}=Q_{ct}-Q_{ca}*Y \quad (9)$$

155 where Q_{ca} is the adsorption capacity of demineralized biochars (mg g^{-1}) and Y is the yield of
156 demineralized biochar from untreated biochar.
157 (ii) Q_{cme} was estimated by the net release of cations (K^+, Ca^{2+}, Na^+, Mg^{2+}) in solution before
158 and after adsorption (Eq. (10)).

$$Q_{cme}=Q_k+Q_{Ca}+Q_{Na}+Q_{Mg} \quad (10)$$

159 where Q_k, Q_{Ca}, Q_{Na}, Q_{Mg} are the adsorption capacity by net release amount of K^+, Ca^{2+}, Na^+
160 and Mg^{2+} during the Cd adsorption process, respectively (mg g^{-1}).
161 (iii) Cd^{2+} sorption on minerals was the result of interaction between ion exchange and mineral
162 precipitation, so Q_{cmp} could be obtained by the difference between Q_{cm} and Q_{cme} value:

$$Q_{cmp}=Q_{cm}-Q_{cme} \quad (11)$$

163 (iv) Q_{co} was calculated by the difference in the pH value of demineralized biochars before and
164 after the adsorption :

$$Q_{co}=Q_{co1}*Y \quad (12)$$

where Q_{co1} is the Cd^{2+} adsorption capacity by complexation with functional groups on demineralized biochars (mg g^{-1}).

(v) Cd^{2+} absorption on demineralized biochars was the result of interaction between Cd^{2+}-π interaction and functional group complexation, so $Q_{c\pi}$ could be obtained by the Q_{ca} value deducted the Q_{co} value:

$$Q_{c\pi} = Q_a * Y - Q_{co} \quad (13)$$

2.6. Statistical analysis

All the experiments were conducted in triplicates. Test data are expressed as mean ± standard deviation and use Origin 2020b software to draw graphics. The significant difference was compared with the least square mean student's t ($P < 0.05$) by JMP 11.0 (two-tailed).

3. Results

3.1. Cd^{2+} absorption on biochars

3.1.1. Kinetics of Cd^{2+} absorption on biochars

The Cd adsorption kinetics were presented in Fig. 1 and Table 1. SBB reached the maximum adsorption capacity within 8h. Compared with SBB, Ca-SBB had a faster adsorption rate for Cd and reached equilibrium within a few minutes (Fig. 1a). Similarly, the Cd^{2+} absorption on Ca-RSB raised rapidly in the first 30 min and reached adsorption equilibrium faster than RSB (Fig. 1b).

The pseudo second order kinetic model matched the kinetic adsorption process of the tested biochars better with the highest R^2 value ($0.974 \leq R^2 \leq 0.999$) (Table 1). The pseudo second order rate constant (k_2) for Ca-SBB and Ca-RSB were 1117 times and 34 times higher than that for SBB and RSB, respectively.

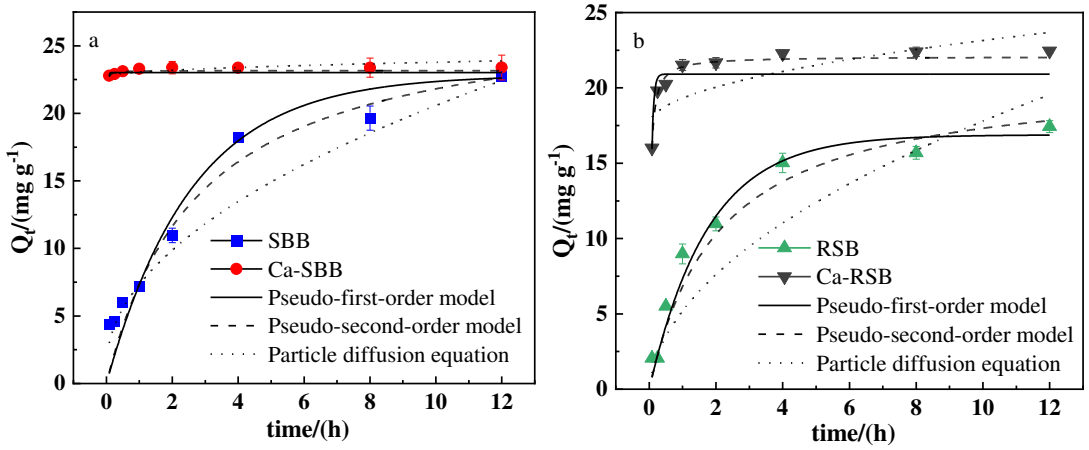

186

187 **Fig. 1** Sorption kinetic of Cd^{2+} on SBB, Ca-SBB (**a**) and RSB, Ca-RSB (**b**), respectively. Q_t

188 (mg g^{-1}) is the amount of metal adsorbed per unit weight of adsorbent

189 Table 1 The regression parameter of kinetics equation for the adsorption of Cd^{2+} onto biochars

Biochars	Pseudo-first-order model			Pseudo-second-order model			Particle diffusion equation	
	Q_e	k_1	R^2	Q_e	k_2	R^2	k_p	R^2
	mg g^{-1}	h^{-1}		mg g^{-1}	g mg^{-1} h^{-1}		mg g^{-1} $h^{-0.5}$	
SBB	24.07	0.356	0.986	26.98	0.016	0.997	6.86	0.983
RSB	16.33	0.509	0.965	18.51	0.040	0.974	5.24	0.927
Ca-SBB	23.31	38.50	0.445	23.34	17.87	0.999	0.824	0.561
Ca-RSB	21.58	15.60	0.831	22.28	1.343	0.981	1.40	0.548

190 Note: Qe are the calculated data (mg g^{-1}); k_1, k_2, k_p is the rate constant for pseudo-first-order model

191 (h^{-1}), pseudo-second-order model (g mg^{-1} h^{-1}) and particle diffusion equation (mg g^{-1} $h^{-0.5}$)

192

193 3.1.2. Isotherms of Cd^{2+} sorption on biochars

194 The adsorption isotherms of Cd^{2+} were illustrated in Fig. 2. At low Cd^{2+} concentrations, a sharp

195 slope appeared. After that, the biochars became saturated reaching steady state conditions.

196 The fitted parameters reported in Table 2 indicated that, the equilibrium sorption data of SBB

and Ca-SBB well fitted to the Langmuir model with R^2 values than the Freundlich model. In particular, the Q_{max} value for Ca-SBB was 1.56 times larger than that for SBB. However, in the cases of the biochar samples RSB and Ca-RSB, both the Langmuir and Freundlich models display high R^2 (>0.98) values. The Langmuir maximum sorption quantity (Q_{max}) of Cd^{2+} for Ca-RSB was about 1.48 times greater than that for RSB.

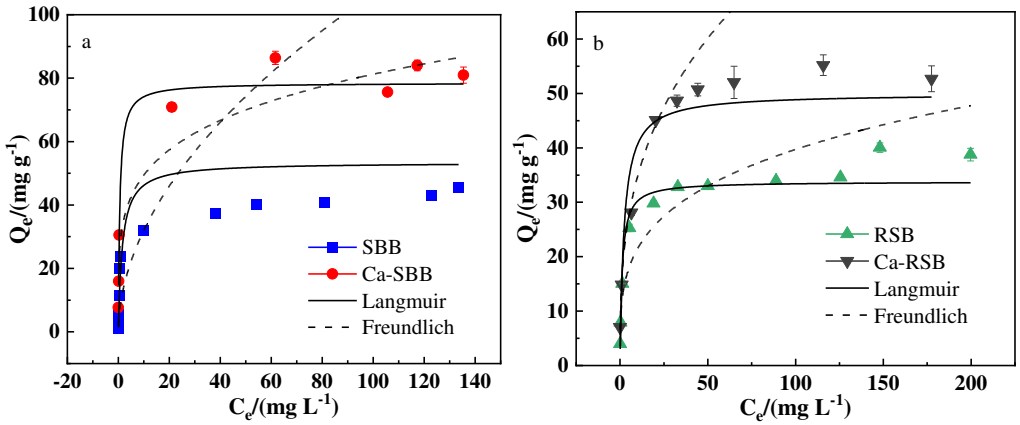

Fig. 2 Sorption isotherm of Cd^{2+} on SBB, Ca-SBB (**a**) and RSB, Ca-RSB (**b**), respectively. Q_e (mg g^{-1}) is the absorption capacity at equilibrium; C_e (mg L^{-1}) is the equilibrium solution concentration

Table 2 The regression parameters of Langmuir and Freundlich models for adsorption isotherm of Cd^{2+} onto biochars

Biochars	Langmuir parameters			Freundlich parameters		
	Q_{max} mg g^{-1}	B L mg^{-1}	R^2	1/n	K	R^2
SBB	50.40	0.641	0.959	0.52	9.59	0.601
RSB	33.79	0.845	0.996	0.27	11.63	0.994

Ca-SBB	78.49	1.70	0.983	0.22	30.09	0.941
Ca-RSB	49.96	0.435	0.990	0.34	15.86	0.983

Note: Q_{max} is the maximum adsorption capacity (mg g^{-1}); B is the Langmuir constant concerned with the Cd absorption energy (L mg^{-1}); N is the Freundlich constant concerned with surface heterogeneity; K is the Freundlich constant concerned with the Cd absorption capacity

3.1.3. Desorption

The distribution of desorption rates of Cd^{2+} was illustrated in Fig. 3. Compared to SBB and RSB, the average desorption efficiencies for Ca-SBB and Ca-RSB obtained with 0.1 mol L^{-1} $NaNO_3$ solution specifically decreased by 97.4% and 98.2%, respectively.

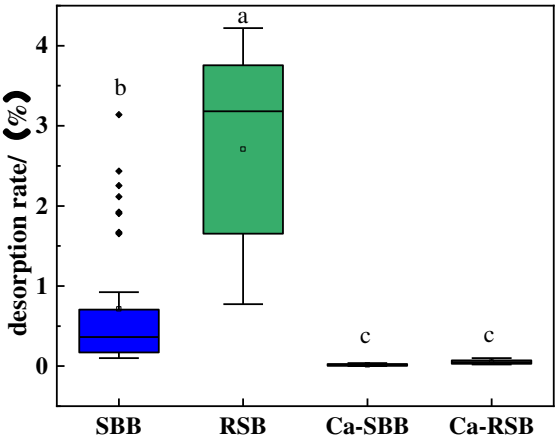

Fig. 3 The distribution of desorption rates of Cd^{2+} onto biochars

3.2. Relative distribution of adsorption mechanisms

As shown in Table 3 and Fig. 4, Q_{cmp} formed the biggest fraction in SBB, followed by Q_{co} and Q_{cme}, with 43.24%, 25.93% and 21.14% compared to the total adsorption, respectively. Conversely, Q_{cme} accounted for the largest part in RSB, followed by Q_{cmp} , with 43.00% and 31.69% in comparison with the total adsorption, respectively. After $Ca(OH)_2$ modification, the Q_{cme} value of Ca-SBB and Ca-RSB specifically increased by 162.0% and 217.4% compared to SBB and RSB, respectively. The contribution of Q_{cme} to the total absorption of Ca-SBB and Ca-RSB increased from

21.14% and 43.00% to 34.93% and 61.91%, respectively. Moreover, Q_{cmp} of Ca-SBB was the dominant value, since it increased by 82.73% compared to SBB. However, Q_{cmp} value of Ca-RSB decreased by 23.50% compared to RSB. Furthermore, Q_{co} value of Ca-SBB and Ca-RSB decreased by 13.14% and 15.74% compared to SBB and RSB, respectively. Still and all, the $Q_{c\pi}$ value of Ca-SBB decreased significantly compared to that of SBB, while the $Q_{c\pi}$ value of Ca-RSB increased significantly compared to that of RSB.

Table 3 Absorption capacity of Cd^{2+} by each mechanism on biochars (mean ± S.D., n=3)

Biochar	Q_{cme} (mg g^{-1})	Q_{cmp} (mg g^{-1})	Q_{co} (mg g^{-1})	$Q_{c\pi}$ (mg g^{-1})
SBB	11.55±0.05d	23.63±0.55b	14.16±0.30a	5.29±0.76a
RSB	19.41±0.20c	14.30±1.79c	8.07±0.15c	3.36±0.10b
Ca-SBB	30.26±0.72b	43.18±0.89a	12.30±0.23b	0.90±0.60c
Ca-RSB	36.66±0.29a	10.94±0.35d	6.80±0.35d	4.81±0.75a

Note: Absorption capacity of Cd^{2+} by ion exchange (Q_{cme}), minerals precipitation (Q_{cmp}), functional groups complexation (Q_{co}) and Cd^{2+}-π coordination ($Q_{c\pi}$) on biochars. Subscripts (a, b, c and d) indicate that the differences in the absorption capacity of Cd^{2+} by each mechanism on biochars in the same treatment is significant ($P<0.05$)

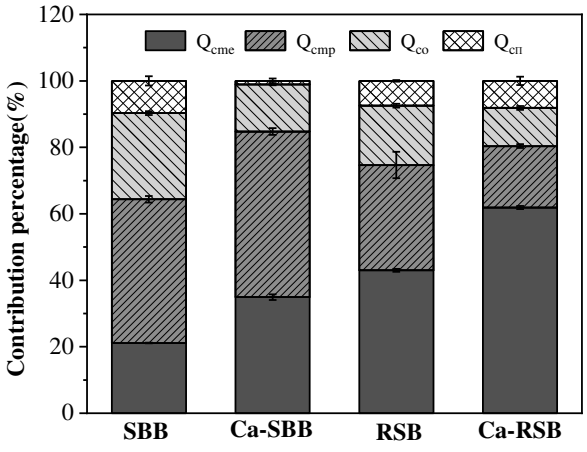

Fig. 4 The contribution percentage of different mechanisms to Cd^{2+} sorption on biochars.

4. Discussion

The isotherm results indicated that SBB had greater adsorption capacity and lower desorption efficiency than RSB. The isotherm adsorption data of SBB conformed to Langmuir model, while that of RSB fitted both Langmuir and Freundlich model. It indicated that the Cd^{2+} adsorption on SBB followed a monolayer absorption mechanism, while on RSB it was not just monolayer, but it followed a multilayer absorption (Li, et al. 2017). The Freundlich constant 1/n is concerned with the surface inhomogeneity of the adsorbent. When 1/n is less than one, it is good for chemical adsorption, otherwise it is good for physical adsorption(Lin, et al. 2017). Because the 1/n value of RSB was 0.27, chemisorption was dominant in RSB.

In SBB, Q_{cmp} accounts for the largest proportion, followed by Q_{co} and Q_{cme}. Q_{cme} contributed the most to the total adsorption of Cd^{2+} in RSB, followed by Q_{cmp}. The tested biochars were scanned by XRD, SEM-EDS and FTIR before and after Cd^{2+} adsorption. Peaks of $CdCO_3$ were found in XRD after Cd^{2+} adsorption both in SBB and RSB, indicating that the major precipitate was $CdCO_3$ (Fig. 5). Likewise, compared with SBB and RSB, white granular crystals were found in the SEM image of SBB+Cd and RSB+Cd, and elements detected by EDS spectrum mainly included Cd, C,

255 O and Ca (Fig. S1).

256 Metal ions on the surface of the biochar can be directly electrostatically adsorbed, or form
257 complexes with oxygen-containing functional groups (e.g., –COOM+, –OM+, –COOMOOC–, –
258 OMO–), or form precipitates with anions (e.g., CaCO3) (Yang, et al. 2019). These ions could be
259 exchanged with Cd2 + during the sorption process. In RSB, the dominance of K^+ were released,
260 since the proportion of K^+ contribution was 87.0% to Q_{cme} in RSB. The total amount of K in RSB
261 was 3.06 times larger than that in SBB (Table S1). Both XRD (Fig. 5) and SEM-EDS results (Fig.
262 S1) also demonstrated that RSB was rich in K. Similar findings have been reported, suggesting the
263 significance of ions exchange in Cd^{2+} adsorption (Huang, et al. 2020; Zhang, et al. 2015).
264 Remarkably, ion-exchange has been reported to contribute up to 79.5% of Cd sorption by hyacinth
265 biochar (Zhang, et al. 2015) and up to 44.49% by rice-husk biochars (Huang, et al. 2020).

266 In addition, the oxygen-containing functional groups on the surface of biochar can adsorb
267 cadmium through complexation (Xia, et al. 2019). FTIR was adopted to study the changes of
268 functional groups before and after Cd^{2+} adsorption (Fig. S2). In general the large peak at 3400cm^{-1}
269 was H-bonded OH and the intense peak at 1600 cm^{-1} was esters C=O or aromatic C=C. The peak of
270 1090 cm^{-1} was most probably concerned with lignin derivative C-O. In addition, the peak of 1270
271 cm^{-1} was most probably concerned with carboxyl O-H, while the peak at 1385 cm^{-1} was related to
272 phenolic O-H (Drosos, et al. 2014). The carboxyl O-H and phenolic O-H of SBB and RSB decreased
273 after Cd adsorption. Besides, the Cd^{2+} coordination with π-bonds such as -CH and C=C was also
274 the reason for Cd^{2+} adsorption on biochars (Wu, et al. 2019). The peak of 1450cm^{-1} was related to
275 aliphatic C-H and the one of 1350cm^{-1} was possibly attributed to methyl C-H (R-O-CH_3) (Drosos,
276 et al. 2009; Drosos, et al. 2014; Sui, et al. 2020). The contribution of $Q_{c\pi}$ to total absorption of SBB

277 and RSB were 9.69% and 7.44%, respectively (Fig. 4), indicating that Cd^{2+}-π coordination
278 influenced the Cd^{2+} adsorption mechanisms.

279 The isotherm results also indicated that compared with the original biochar (SBB, RSB), alkali-
280 modified biochars (Ca-SBB and Ca-RSB) had greater adsorption capacities, faster adsorption
281 kinetics and lower desorption efficiencies. However, it was interesting that the response mechanism
282 of the two kinds of straw biochars to alkali modification was different.

283 $Ca(OH)_2$ modification both effectively enhanced the adsorption capacity resulted from ion
284 exchange mechanism on SBB and RSB (Table 3 and Fig. 4). Cation exchange capacity (CEC) is a
285 major indicator of Cd^{2+} adsorption when ion exchange is the predominant mechanism(Yang, et al.
286 2019) . Higher CEC was obtained in alkali-modified biochars than the original biochars (Table S1).
287 Consistently, good correlation was observed between Q_{cme} and CEC (Fig. S3). The dominance of
288 Ca^{2+} was found in Ca-SBB and Ca-RSB, since the contribution proportions of Ca^{2+} in Ca-SBB and
289 Ca-RSB were 37.9% , 70.7% to Q_{cme}, respectively, higher than that in SBB and RSB (Table S2).
290 Alkali-modified biochars also contained more Ca than the original biochars (Table S1). Moreover,
291 metal ion exchange formed the biggest fraction in RSB and Ca-RSB. Although $Ca(OH)_2$
292 modification improved the ion exchange effect, the desorption rates of Ca-SBB and Ca-RSB were
293 extremely low (Fig. 3). The reason for this may be due to the fact that the ions exchanged with
294 cadmium derived mainly from organic complexes, containing functional groups, and mineral
295 precipitation rather than from direct electrostatic attraction.

296 After Cd^{2+} adsorption, peaks of $CdCO_3$ were found in Ca-SBB and Ca-RSB (Fig. 5). $CdCO_3$
297 precipitation was also reported by Cui, et al. (2016). Likewise, compared with the original biochar,
298 white granular crystals were observed in the SEM image of Cd-loaded biochars, especially SBB+Cd,

299 Ca-SBB+Cd and Ca-RSB+Cd. elements detected by EDS spectrum mainly included Cd, C, O and
300 Ca (Fig. S1). In addition, minerals precipitation formed the biggest fraction in SBB and Ca-SBB
301 (Table 3 and Fig. 4). $Ca(OH)_2$ modification effectively enhanced the Q_{cmp} value of SBB. However,
302 the Q_{cmp} value of Ca-SBB decreased significantly compared to that of SBB. Differences of Q_{cmp}
303 between SBB and RSB after modification were related to the elemental and mineral composition
304 differences of RSB and SBB. For example, SBB contained more Ca and soluble CO_3^{2-} than RSB,
305 while RSB had more K than SBB (Table S1). The XRD patterns indicated that $CaCO_3$ and $CaHPO_4$
306 were the main crystals in SBB, while KCl and $CaCO_3$ were the main crystals in RSB. After $Ca(OH)_2$
307 modification, the main compound for Ca-SBB was $CaCO_3$, while for Ca-RSB the main compounds
308 were both $CaCO_3$ and KCl (Fig. 5). SBB had higher pH than RSB. $Ca(OH)_2$ modification effectively
309 enhanced the pH value of SBB, but had no significant effect on RSB (Table S1). The pH value is an
310 important indicator of Q_{cmp} . Consistently, good correlation was observed between Q_{cmp} and pH (Fig.
311 S4).

312 $Ca(OH)_2$ modification remarkably decreased Q_{co} because of the changes of functional groups
313 such as -OH, and –COOH (Fig. S2). Ca-SBB had less carboxylic OH than SBB, since Ca would
314 bind carboxyl groups. However, it had more phenolic OH than SBB, which revealed structural
315 differences due to the alkali modification. Ca-RSB had less carboxylic OH and phenolic OH than
316 RSB, which showed a difference in structure from SBB and also different mechanism of the biochar
317 formation due to the $Ca(OH)_2$ modification. After the Cd^{2+} interaction, the band intensities of
318 carboxylic OH as well as phenolic OH were decreased for SBB, Ca-SBB and RSB. Therefore,
319 functional groups such as -OH, and -COOH, seem to be mainly responsible for Cd^{2+} complexation.
320 However, following Cd absorption in Ca-RSB, only the band intensity of phenolic OH was

decreased, while carboxylic OH was not further reduced. This finding suggested that Cd application may result in Ca desorption and Cd adsorption in the material but the overall carboxylate binding balance remained unchanged. This result was in line with the adsorption mechanism presented in Table 3, which showed that cation exchange was the main mechanism of Cd binding in Ca-RSB (36.66 mg g^{-1}). The contribution of $Q_{c\pi}$ to the total absorption of the tested biochars was in the range of 1.02% to 9.06% (Fig. 4), indicating that Cd^{2+}-π coordination influenced the Cd^{2+} adsorption. As a matter of fact, $Q_{c\pi}$ value of Ca-SBB was much lower than that of Ca-RSB (Table 3). The reason for this change was the chemical alteration of RSB after modification as revealed by the C/N ratio differences between RSB and Ca-RSB (Table S1). Actually the C/N ratio for Ca-RSB was almost 2.6 times higher than that of RSB (Table S1).High C/N ratio is the result of a hydrophobic material, not accessible to microbial decay (Brust 2019).

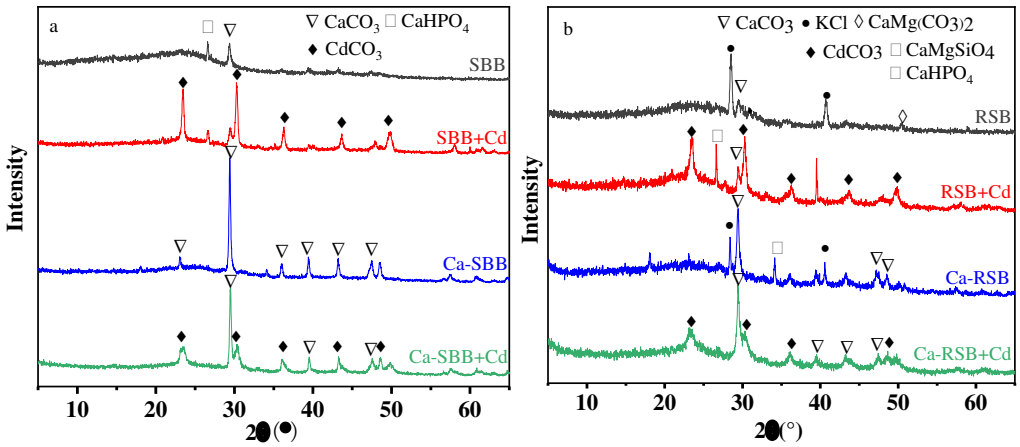

Fig. 5 XRD spectra of SBB, Ca-SBB (**a**) and RSB, Ca-RSB (**b**) before and after Cd^{2+} adsorption, respectively

5. Conclusions

Compared with the original biochar (SBB, RSB), alkali-modified biochars (Ca-SBB and Ca-RSB) had greater adsorption capacities, faster adsorption rates and lower desorption efficiencies.

The Cd^{2+} absorption mechanism of the tested biochars mainly included mineral co-precipitation, ion exchange, complexation with functional groups and Cd^{2+}-π coordination. Ion exchange and precipitation mechanisms dominated Cd^{2+} sorption on RSB, while precipitation and functional groups complexation mechanisms dominated Cd^{2+} sorption on SBB. After $Ca(OH)_2$ modification, the interaction between Cd^{2+} and minerals (precipitation and ion exchange) was the main Cd^{2+} adsorption mechanism on alkali-modified biochars (Ca-SBB, Ca-RSB). Also, the response mechanism of the two kinds of straw biochars to alkali modification was different. These findings suggest that alkali-modified biochars exhibit a great potential for heavy metal remediation.

Ethical approval

The authors declare that the submitted manuscript is original and unpublished elsewhere, and that this manuscript complies with the Ethical Rules applicable for this journal.

Consent to participate

All participants have been involved directly or indirectly in the research itself.

Consent to publish

All the authors listed in the manuscript have agreed for authorship, read, and approved the manuscript and given consent for submission and subsequent publication of the manuscript. The order of authorship has been approved by all named authors prior to submission, and the name of the corresponding author has been agreed by all the authors.

Authors contributions

Yaxin Kang: Conceptualization, Software, Investigation, Data Curation, Formal analysis , Visualization, Writing - Original Draft. Yi Zhou: Investigation, Resources. Hao Li: Investigation. Shanguo Chen: Investigation. Fenghua Tian: Investigation. Lianqing Li: Methodology, Validation ,Writing - Review & Editing, Funding acquisition, Project administration. Marios Drosos: Writing - Review & Editing, Formal analysis. Genxing Pan: Supervision. Stephen Joseph: Formal analysis.

Funding

This study was financially supported by the National Natural Science Foundation of China (NSFC) (42077148), the National Key Research and Development Program of China (2016YFD0800306).

Competing interests

The authors declare no conflict of interest.

Availability of data and materials

All data generated or analyzed during this study are included in this manuscript and its supplementary information files. All the materials used during the current study are available from the corresponding author on reasonable request.

References

383 Ahmad M, Rajapaksha A U, Lim J E, Zhang M, Bolan N, Mohan D, Vithanage M, Lee S S, Ok Y S (2014)
384 Biochar as a sorbent for contaminant management in soil and water: A review. Chemosphere 99:
385 19-33. http://dx.doi.org/10.1016/j.chemosphere.2013.10.071
386 Ahmed M B, Zhou J L, Ngo H H, Guo W, Chen M (2016) Progress in the preparation and application of
387 modified biochar for improved contaminant removal from water and wastewater. Bioresour.
388 Technol. 214: 836-851. http://dx.doi.org/10.1016/j.biortech.2016.05.057
389 Bian R J, Joseph S, Cui L Q, Pan G X, Li L Q, Liu X Y, Zhang A, Rutlidge H, Wong S W, Chia C, Marjo
390 C, Gong B, Munroe P, Donne S (2014) A three-year experiment confirms continuous
391 immobilization of cadmium and lead in contaminated paddy field with biochar amendment. J.
392 Hazard. Mater. 272: 121-128. http://dx.doi.org/10.1016/j.jhazmat.2014.03.017
393 Bolan N, Kunhikrishnan A, Thangarajan R, Kumpiene J, Park J, Makino T, Kirkham M B, Scheckel K
394 (2014) Remediation of heavy metal(loid)s contaminated soils - To mobilize or to immobilize? J.
395 Hazard. Mater. 266: 141-166. http://dx.doi.org/10.1016/j.jhazmat.2013.12.018
396 Brust G E (2019) Management Strategies for Organic Vegetable Fertility. In: Biswas, D and Micallef, S
397 A (ed) Safety and Practice for Organic Food. Academic Press, pp 193-212
398 Burakov A E, Galunin E V, Burakova I V, Kucherova A E, Agarwal S, Tkachev A G, Gupta V K (2018)
399 Adsorption of heavy metals on conventional and nanostructured materials for wastewater
400 treatment purposes: A review. Ecotox. Environ. Safe. 148: 702-712.
401 http://dx.doi.org/10.1016/j.ecoenv.2017.11.034
402 Cui X, Fang S, Yao Y, Li T, Ni Q, Yang X, He Z (2016) Potential mechanisms of cadmium removal from
403 aqueous solution by Canna indica derived biochar. Sci. Total Environ. 562: 517-525.
404 http://dx.doi.org/10.1016/j.scitotenv.2016.03.248
405 Drosos M, Jerzykiewicz M, Deligiannakis Y (2009) H-binding groups in lignite vs. soil humic acids:
406 NICA-Donnan and spectroscopic parameters. J. Colloid Interface Sci. 332(1): 78-84.
407 http://dx.doi.org/10.1016/j.jcis.2008.12.023
408 Drosos M, Leenheer J A, Avgeropoulos A, Deligiannakis Y (2014) H-binding of size- and polarity-
409 fractionated soil and lignite humic acids after removal of metal and ash components. Environ. Sci.
410 Pollut. Res. 21(5): 3963-3971. http://dx.doi.org/10.1007/s11356-013-2302-9
411 Fu F L, Wang Q (2011) Removal of heavy metal ions from wastewaters: A review. J. Environ. Manage.

92(3): 407-418. http://dx.doi.org/10.1016/j.jenvman.2010.11.011

Gaskin J W, Steiner C, Harris K, Das K C, Bibens B (2008) EFFECT OF LOW-TEMPERATURE PYROLYSIS CONDITIONS ON BIOCHAR FOR AGRICULTURAL USE. Trans. ASABE 51(6): 2061-2069.

Huang F, Gao L-Y, Wu R-R, Wang H, Xiao R-B (2020) Qualitative and quantitative characterization of adsorption mechanisms for Cd2+ by silicon-rich biochar. Sci. Total Environ. 731. http://dx.doi.org/10.1016/j.scitotenv.2020.139163

Inyang M I, Gao B, Yao Y, Xue Y W, Zimmerman A, Mosa A, Pullammanappallil P, Ok Y S, Cao X D (2016) A review of biochar as a low-cost adsorbent for aqueous heavy metal removal. Crit. Rev. Environ. Sci. Technol. 46(4): 406-433. http://dx.doi.org/10.1080/10643389.2015.1096880

Lehmann J (2007) Bio-energy in the black. Front. Ecol. Environ. 5(7): 381-387. http://dx.doi.org/10.1890/1540-9295(2007)5[381:bitb]2.0.co;2

Lehmann J (2007) A handful of carbon. Nature 447(7141): 143-144. http://dx.doi.org/10.1038/447143a

Li B, Yang L, Wang C-q, Zhang Q-p, Liu Q-c, Li Y-d, Xiao R (2017) Adsorption of Cd(II) from aqueous solutions by rape straw biochar derived from different modification processes. Chemosphere 175: 332-340. http://dx.doi.org/10.1016/j.chemosphere.2017.02.061

Li H, Dong X, da Silva E B, de Oliveira L M, Chen Y, Ma L Q (2017) Mechanisms of metal sorption by biochars: Biochar characteristics and modifications. Chemosphere 178: 466-478. http://dx.doi.org/10.1016/j.chemosphere.2017.03.072

Lin L N, Qiu W W, Wang D, Huang Q, Song Z G, Chau H W (2017) Arsenic removal in aqueous solution by a novel Fe-Mn modified biochar composite: Characterization and mechanism. Ecotox. Environ. Safe. 144: 514-521. http://dx.doi.org/10.1016/j.ecoenv.2017.06.063

Patar A, Giri A, Boro F, Bhuyan K, Singha U, Giri S (2016) Cadmium pollution and amphibians - Studies in tadpoles of Rana limnocharis. Chemosphere 144: 1043-1049. http://dx.doi.org/10.1016/j.chemosphere.2015.09.088

Ren N, Tang Y, Li M (2018) Mineral additive enhanced carbon retention and stabilization in sewage sludge-derived biochar. Process Saf. Environ. Prot. 115: 70-78. http://dx.doi.org/10.1016/j.psep.2017.11.006

Sui F, Wang J, Zuo J, Joseph S, Munroe P, Drosos M, Li L, Pan G (2020) Effect of amendment of biochar

441 supplemented with Si on Cd mobility and rice uptake over three rice growing seasons in an acidic
442 Cd-tainted paddy from central South China. Sci. Total Environ. 709.
443 http://dx.doi.org/10.1016/j.scitotenv.2019.136101
444 Tan X F, Liu Y G, Gu Y L, Xu Y, Zeng G M, Hu X J, Liu S B, Wang X, Liu S M, Li J (2016) Biochar-
445 based nano-composites for the decontamination of wastewater: A review. Bioresour. Technol. 212:
446 318-333. http://dx.doi.org/10.1016/j.biortech.2016.04.093
447 Trakal L, Bingol D, Pohorely M, Hruska M, Komarek M (2014) Geochemical and spectroscopic
448 investigations of Cd and Pb sorption mechanisms on contrasting biochars: Engineering
449 implications. Bioresour. Technol. 171: 442-451. http://dx.doi.org/10.1016/j.biortech.2014.08.108
450 Wang R Z, Huang D L, Liu Y G, Zhang C, Lai C, Zeng G M, Cheng M, Gong X M, Wan J, Luo H (2018)
451 Investigating the adsorption behavior and the relative distribution of Cd2+ sorption mechanisms
452 on biochars by different feedstock. Bioresour. Technol. 261: 265-271.
453 http://dx.doi.org/10.1016/j.biortech.2018.04.032
454 Wang Z, Liu G, Zheng H, Li F, Ngo H H, Guo W, Liu C, Chen L, Xing B (2015) Investigating the
455 mechanisms of biochar's removal of lead from solution. Bioresour. Technol. 177: 308-317.
456 http://dx.doi.org/10.1016/j.biortech.2014.11.077
457 Wilson K, Yang H, Seo C W, Marshall W E (2006) Select metal adsorption by activated carbon made
458 from peanut shells. Bioresour. Technol. 97(18): 2266-2270.
459 http://dx.doi.org/10.1016/j.biortech.2005.10.043
460 Woods W I, Falcao N P S, Teixeira W G (2006) Biochar trials aim to enrich soil for smallholders. Nature
461 443(7108): 144-144. http://dx.doi.org/10.1038/443144b
462 Wu J W, Wang T, Zhang Y S, Pan W P (2019) The distribution of Pb(II)/Cd(II) adsorption mechanisms
463 on biochars from aqueous solution: Considering the increased oxygen functional groups by HCl
464 treatment. Bioresour. Technol. 291: 7. http://dx.doi.org/10.1016/j.biortech.2019.121859
465 Xia Y, Yang T, Zhu N, Li D, Chen Z, Lang Q, Liu Z, Jiao W (2019) Enhanced adsorption of Pb(II) onto
466 modified hydrochar: Modeling and mechanism analysis. Bioresour. Technol. 288.
467 http://dx.doi.org/10.1016/j.biortech.2019.121593
468 Yang X D, Wan Y S, Zheng Y L, He F, Yu Z B, Huang J, Wang H L, Ok Y S, Jiang Y S, Gao B (2019)
469 Surface functional groups of carbon-based adsorbents and their roles in the removal of heavy

metals from aqueous solutions: A critical review. Chem. Eng. J. 366: 608-621. http://dx.doi.org/10.1016/j.cej.2019.02.119

Yu W C, Lian F, Cui G N, Liu Z Q (2018) N-doping effectively enhances the adsorption capacity of biochar for heavy metal ions from aqueous solution. Chemosphere 193: 8-16. http://dx.doi.org/10.1016/j.chemosphere.2017.10.134

Zhang A F, Cui L Q, Pan G X, Li L Q, Hussain Q, Zhang X H, Zheng J W, Crowley D (2010) Effect of biochar amendment on yield and methane and nitrous oxide emissions from a rice paddy from Tai Lake plain, China. Agric. Ecosyst. Environ. 139(4): 469-475. http://dx.doi.org/10.1016/j.agee.2010.09.003

Zhang F, Wang X, Yin D X, Peng B, Tan C Y, Liu Y G, Tan X F, Wu S X (2015) Efficiency and mechanisms of Cd removal from aqueous solution by biochar derived from water hyacinth (Eichornia crassipes). J. Environ. Manage. 153: 68-73. http://dx.doi.org/10.1016/j.jenvman.2015.01.043

Figures

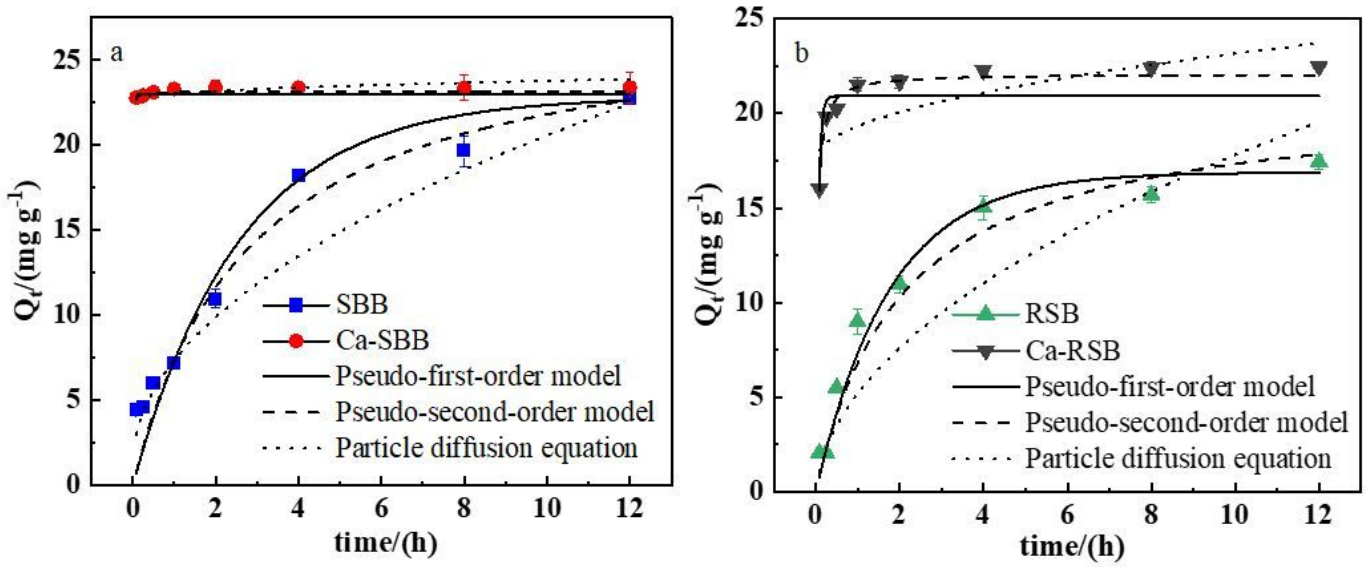

Figure 1

Sorption kinetic of Cd2+ on SBB, Ca-SBB (a) and RSB, Ca-RSB (b), respectively. Qt (mg g-1) is the amount of metal adsorbed per unit weight of adsorbent

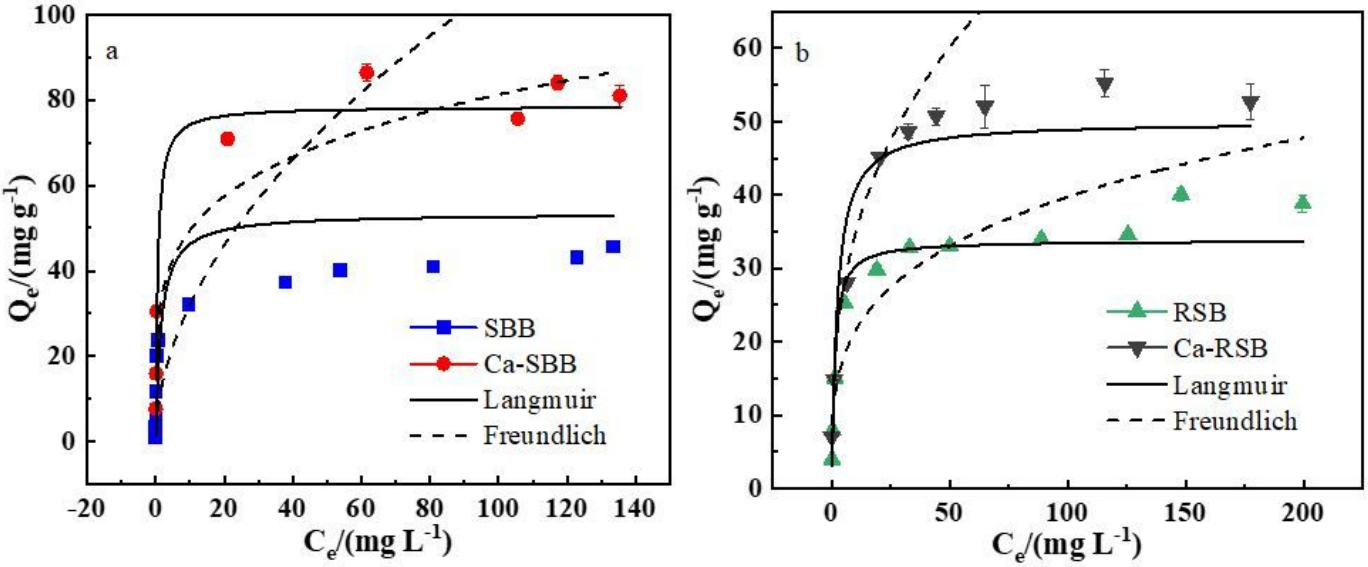

Figure 2

Sorption isotherm of Cd2+ on SBB, Ca-SBB (a) and RSB, Ca-RSB (b), respectively. Qe (mg g-1) is the absorption capacity at equilibrium; Ce (mg L-1) is the equilibrium solution concentration

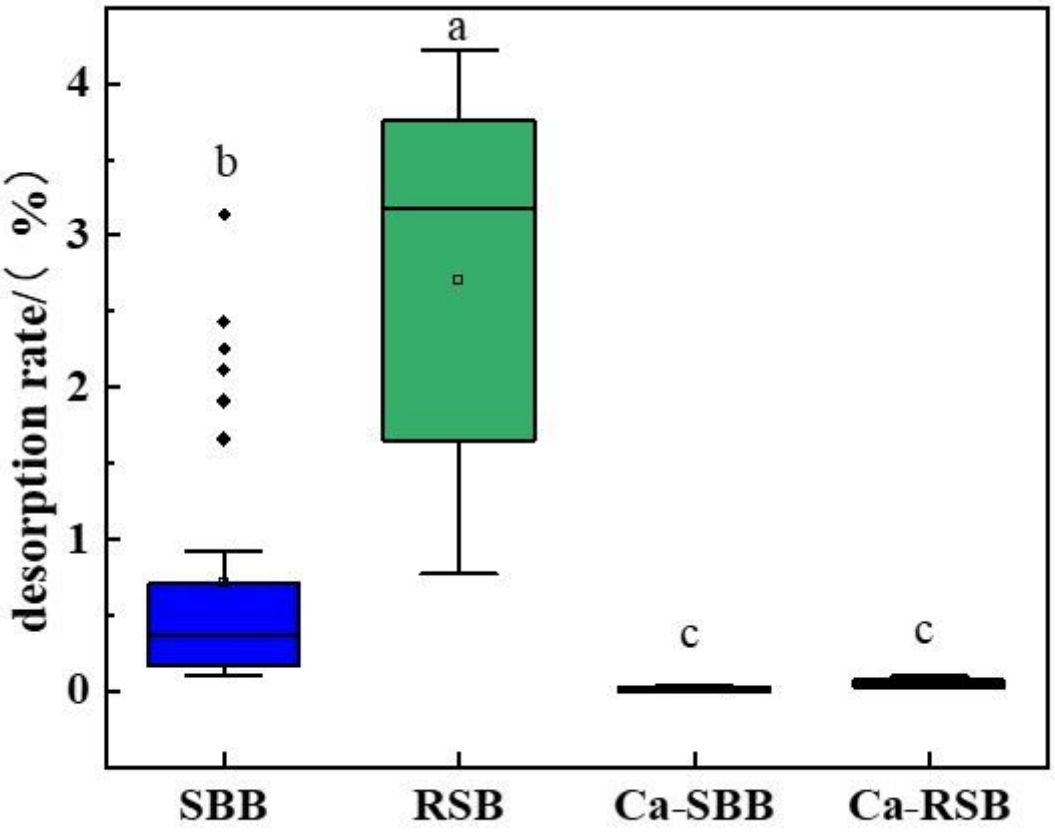

Figure 3

The distribution of desorption rates of Cd2+ onto biochars

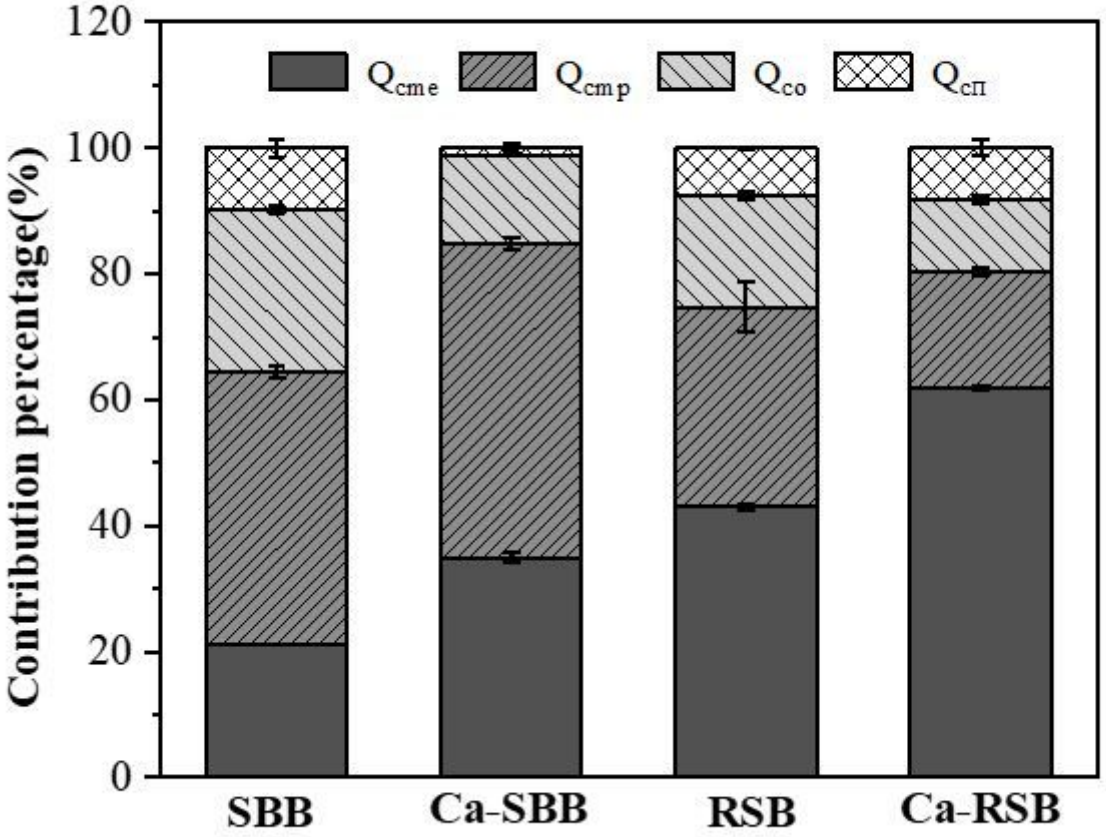

Figure 4

The contribution percentage of different mechanisms to Cd2+ sorption on biochars.

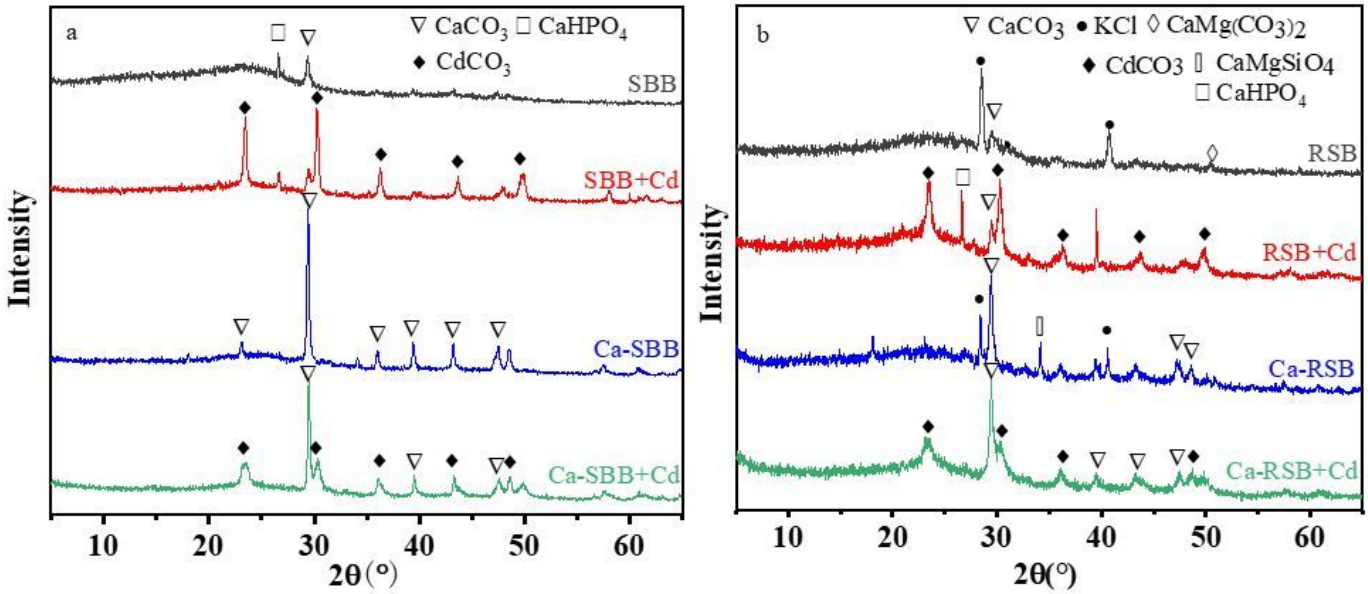

Figure 5

XRD spectra of SBB, Ca-SBB (a) and RSB, Ca-RSB (b) before and after Cd2+ adsorption, respectively

Supplementary Files

This is a list of supplementary files associated with this preprint. Click to download.

- Supplementarymaterial.docx